

PAPER • OPEN ACCESS

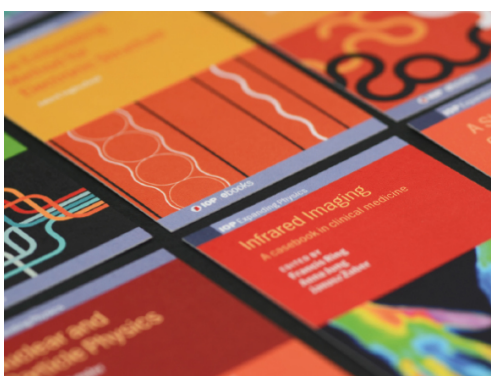
Effects of off-axis translocation through nanopores on the determination of shape and volume estimates for individual particles

To cite this article: Cuifeng Ying *et al* 2022 *Nanotechnology* **33** 275501

View the [article online](#) for updates and enhancements.

You may also like

- [Wafer-level fabrication of individual solid-state nanopores for sensing single DNAs](#)
Hithesh K Gatty, Nguyen Xuan Chung, Miao Zhang *et al.*
- [DNA motion induced by electrokinetic flow near an Au coated nanopore surface as voltage controlled gate](#)
Manabu Sugimoto, Yuta Kato, Kentaro Ishida *et al.*
- [Manipulation of DNA transport through solid-state nanopores by atomic force microscopy](#)
Wei Si, Haojie Yang, Gensheng Wu *et al.*



IOP | ebooks™

Bringing together innovative digital publishing with leading authors from the global scientific community.

Start exploring the collection—download the first chapter of every title for free.

Effects of off-axis translocation through nanopores on the determination of shape and volume estimates for individual particles

Cuifeng Ying^{1,2,*} , Jared Houghtaling¹  and Michael Mayer^{1,*} 

¹ Adolphe Merkle Institute, University of Fribourg, Fribourg, Switzerland

² Advanced Optics and Photonics Laboratory, Department of Engineering, School of Science & Technology, Nottingham Trent University, Nottingham, United Kingdom

E-mail: cuifeng.ying@ntu.ac.uk and michael.mayer@unifr.ch

Received 24 January 2022, revised 15 March 2022

Accepted for publication 22 March 2022

Published 12 April 2022



CrossMark

Abstract

Resistive pulses generated by nanoparticles that translocate through a nanopore contain multi-parametric information about the physical properties of those particles. For example, non-spherical particles sample several different orientations during translocation, producing fluctuations in blockade current that relate to their shape. Due to the heterogenous distribution of electric field from the center to the wall of a nanopore while a particle travels through the pore, its radial position influences the blockade current, thereby affecting the quantification of parameters related to the particle's characteristics. Here, we investigate the influence of these off-axis effects on parameters estimated by performing finite element simulations of dielectric particles transiting a cylindrical nanopore. We varied the size, ellipsoidal shape, and radial position of individual particles, as well as the size of the nanopore. As expected, nanoparticles translocating near the nanopore wall produce increase current blockades, resulting in overestimates of particle volume. We demonstrated that off-axis effects also influence estimates of shape determined from resistive pulse analyses, sometimes producing a multiple-fold deviation in ellipsoidal length-to-diameter ratio between estimates and reference values. By using a nanopore with the minimum possible diameter that still allows the particle to rotate while translocating, off-axis effects on the determination of both volume and shape can be minimized. In addition, tethering the nanoparticles to a fluid coating on the nanopore wall makes it possible to determine an accurate particle shape with an overestimated volume. This work provides a framework to select optimal ratios of nanopore to nanoparticle size for experiments targeting free translocations.

Supplementary material for this article is available [online](#)

Keywords: off-axis effect, nanopore resistive-pulse sensing, finite element simulation, particle shape

(Some figures may appear in colour only in the online journal)

* Authors to whom any correspondence should be addressed.

 Original content from this work may be used under the terms of the [Creative Commons Attribution 4.0 licence](#). Any further distribution of this work must maintain attribution to the author(s) and the title of the work, journal citation and DOI.

1. Introduction

Resistive pulse-based nanopore sensing relies on the Coulter counting principle [1], where each particle transiting a nanopore displaces highly conductive electrolyte and transiently reduces the ionic current through the pore. The amplitude, duration, and frequency of these resistive pulses

provide information about the size, charge, and concentration of the particles passing through the pore [2–4]. In the past two decades, solid-state nanopores have become an emerging technique for sensing and characterizing of individual biomolecules such as DNA [5–10], proteins [4, 11–14], and viruses [15–17]. Moreover, as a non-spherical particle adopts different orientations within the nanopore, it produces fluctuations in the measured resistive-pulse current that relate to the shape of the particle. For instance, an ellipsoid in its lengthwise orientation blocks the current through a nanopore less than in its crosswise orientation. This effect can be quantified by the electrical shape factor, γ , a descriptor that depends on the particle's ellipsoidal shape, m , and orientation within a cylindrical sensing volume [4, 18–21]. Here, particle shape is approximated as an ellipsoid with axes A , B , B , and $m = A/B$. By comparing the minimum and maximum current values within a resistive pulse as well as the time-dependent change of the current, nanopore sensing makes it possible to characterize proteins with different sizes, shapes, charges, dipole moments, and rotational diffusion coefficients [4, 22–25]. This approach of resistive pulse analysis, however, assumes that the particles translocate along the central axis of a perfectly cylindrical nanopore with a homogenous electrical field, and that the particles are able to rotate freely within the nanopore. When the particles diffuse away from the central axis during their transit through the nanopore, however, they distort the electric field asymmetrically and produce resistive pulse fluctuations that depend on their distance from the central axis [26–29], as well as on their orientation. Computational studies of resistive pulses at the microscale showed a distinct increase in pulse amplitude caused by this off-axis translocation, resulting in the measurement of an inaccurately large volume for spherical particles [27, 28]. By combining the analysis of resistive pulses with optical measurements in a microfluidic platform, Hinkle *et al* confirmed experimentally the correlation between the particles' off-axis position with the amplitude of the resistive pulse [29]. At the nanoscale, such as in the case of nanopore sensing, the increases in the pulse amplitude can be of the same order of magnitude as the system noise. Therefore, the off-axis effect not only leads to an overestimation of volume, but also increases the uncertainty of the volume and shape estimation. Specifically, the fluctuations produced when a spherical particle diffuses laterally within the pore appear similar to those of a rotating non-spherical particle passing through the center of a nanopore. It is therefore important to quantify the effects of off-axis translocation on resistive-pulse measurements, especially in the context of characterizing mixtures of proteins or examining transient changes in a protein population.

Here, we determine the effects of off-axis translocation in the context of ellipsoidal nanoparticles in a cylindrical nanopore using finite element simulations (COMSOL Multiphysics 5.2a). We performed a wide parameter sweep, varying the radial position of individual particles as well as the ratio of particle size to nanopore radius. We further examined the effects of off-axis translocation on the estimation of protein shape by considering particles with a fixed volume but with different shapes, at different radial positions and

rotational orientations. The results reveal that (1) off-axis effects increase as the diameter of the nanopore grows in relation to the diameter of the particle, (2) ellipsoidal particles with length-to-diameter ratios further from a sphere elicit larger, and orientation-dependent, off-axis effects than spherical particles of the same volume, and (3) off-axis effects add a noise-like element to resistive pulse recordings that can produce errors in estimates of length-to-diameter ratio and volume.

2. Analysis methods

2.1. Resistive-pulse sensing analyses based on ohm's law

Resistive-pulse nanopore sensing monitors ion flux through a sensing volume—here, the nanopore channel—in the presence and absence of non-conducting particles. The principle is straightforward when considering the electrolyte as a homogeneous conductive medium with resistivity ρ . The resistance of a cylindrical nanopore with diameter of d_p and length of l_p consists of two components: resistance to ions passing through the confines of the pore itself, R_{pore} , and access resistance of ionic current paths converging to the entrance and from the exit of the pore, R_{access} . One commonly used analytical equation for modelling the total resistance of a cylindrical nanopore, R_{total} , can be written as [30]

$$R_{total} = R_{pore} + R_{access} = \rho \left(\frac{4l_p}{\pi d_p^2} + \frac{1}{d_p} \right) = \rho \left(\frac{l_p + \frac{\pi}{4}d_p}{\frac{\pi}{4}d_p^2} \right). \quad (1)$$

For resistive pulse-based analysis of data obtained with cylindrical nanopores, the electric field is considered to be uniform along the effective nanopore length, l_{eff} , with a net electric field strength of $E = V/l_{eff}$ [31]. Here $l_{eff} = l_p + \frac{\pi}{4}d_p$ as implied by equation (1). We relate the volume of the particle, Λ , and the shape- and angle-dependent electrical shape factor, γ , to the magnitude of the current blockade through the following equation [4, 22]

$$\frac{\Delta I}{I_0} = \frac{4\gamma\Lambda}{\pi d_p^2 \left(l_p + \frac{\pi}{4}d_p \right)}. \quad (2)$$

Here ΔI is the magnitude of the current change induced by a particle translocation, and I_0 is the current of the nanopore in the absence of the particle. For a perfect sphere, γ is 1.5. Therefore, the normalised magnitude of the resistive pulse, $\Delta I/I_0$, is proportional to the volume of the translocating particle. Non-spherical particles have a maximum electrical shape factor, γ_{max} , and a minimum electrical shape factor, γ_{min} , as shown in figure 1(a). These two extreme shape factors generate resistive pulses that fluctuate between $\Delta I_{min} = \frac{4\gamma_{min}\Lambda}{\pi d_p^2 \left(l_p + \frac{\pi}{4}d_p \right)} I_0$ and $\Delta I_{max} = \frac{4\gamma_{max}\Lambda}{\pi d_p^2 \left(l_p + \frac{\pi}{4}d_p \right)} I_0$ [4]. The electric field produces a torque on non-spherical particles with a permanent dipole moment that may bias them toward either a minimum or maximum orientation [4, 22]. With the probability distribution of γ , we can determine the shape and

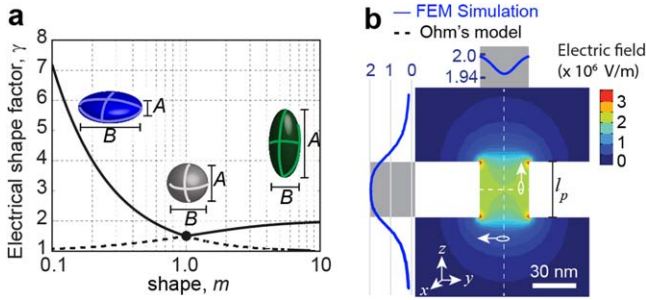


Figure 1. Schematical illustration of shape determination by resistive pulse-based nanopore sensing. (a) The electrical shape factor, γ , as a function of a particle's length-to-diameter ratio, m [20]. The solid curve represents the maximum electrical shape factor γ_{\max} . The dashed curve represents the minimum electrical shape factor γ_{\min} . (b) The distribution of electric field strength in the nanopore determined by finite element simulation. The gray boxes at the left and top represent the nanopore channel. The blue curves represent the simulated electric field strength on the lateral and transverse axes indicated by white dashed lines.

volume as fitting parameters by using an iterative convolution fitting procedure, described previously in supplementary note 1 of [22]. Note that this consideration is only suitable when the diameter of the particle, d_{particle} , is smaller than the diameter of the nanopore (e.g. $d_{\text{particle}}/d_p < 0.5$). When the particle approaches the diameter of the nanopore, the electric field distribution becomes non-uniform, and this model will no longer apply [18].

This model considers that the electric field inside the nanopore is uniform and describes the scenario whereby a particle is located at the center of a large-aspect-ratio, cylindrical nanopore. The mobility of ions in the nanopore is, however, non-uniform as ions cannot diffuse freely near the nanopore wall. In other words, the ohmic medium inside the nanopore is non-homogenous. This heterogeneity leads to deviations from the model when the particle leaves the central axis of the pore and approaches its wall.

2.2. Resistive-pulse sensing analyses based on the PNP function

The Poisson–Nernst–Planck (PNP) equations are commonly used to express the flow of ionic current through a nanopore [29, 32–38]. The Poisson function describes the distribution of potentials, Φ , in an electrolyte solution containing ionic species, i (K^+ or Cl^- , in this case), at concentration c_i and charge z_i

$$\nabla^2 \Phi = -\frac{F}{\varepsilon} \sum_i z_i c_i. \quad (3)$$

The Nernst–Planck equation describes the motion of the ions in a fluid medium under an applied external potential by considering the diffusion of ions, D_i [39]

$$\mathbf{J}_i = -D_i \nabla c_i - \frac{z_i F}{RT} D_i c_i \nabla \Phi, \quad (4)$$

where F represents the Faraday constant, ε is the dielectric constant of the fluidic medium, R is the gas constant and T is the absolute temperature. Table 1 lists the constants and

parameters we used in the simulations to solve PNP equations in this work. The total ionic current is the integral of the z component of the total ion fluxes, \mathbf{J}_i , over the cross-sectional area of the nanopore, S

$$I = F \int (z_{\text{K}^+} \mathbf{J}_{\text{K}^+} + z_{\text{Cl}^-} \mathbf{J}_{\text{Cl}^-}) \cdot \mathbf{n} dS \quad (5)$$

where \mathbf{n} is the unit vector in the direction of the z -axis. In comparison to analytical models, numerical simulations of the PNP equations make it possible to incorporate complex parameters including surface charge and curvature at the entrance to the pore, off-axis position of the particles, and complex geometries for both the nanopore and the particles [17, 22, 32, 35, 38, 40, 41].

In this work, we use COMSOL Multiphysics 5.2a to solve the PNP equations. To simulate our experiments for lipid-coated nanopores [4, 22, 40, 42–45], we defined the nanopore length to be 40 nm (30 nm before coating) and the surface charge on the nanopore wall to be zero [46]. We applied 0.1 V across the nanopore containing 2 M KCl. Because the effective ionic transference number (i.e. the fraction of the overall conductance contributed solely by the specific ionic species) is nonlinearly related to salt concentration [39, 47], we used a concentration of 1.68 M KCl instead of 2 M according to the measured conductivity of the solution, as listed in table 1 [40]. Figure 1(b) shows the electric field distribution in a 30 nm diameter nanopore determined by solving the PNP equations. The simulated electric field distributions along the lateral and transverse axes, represented by the blue curves on the left and top, respectively, are not perfectly uniform inside the nanopore.

3. Results and discussion

3.1. Off-axis position modulates resistive-pulse amplitudes

A particle that passes through a nanopore near the pore wall produces a larger resistive pulse than that same particle passing through the center of the pore [26–28, 48]. Figure 2 and supplementary video 1 (available online at stacks.iop.org/NANO/33/275501/mmedia) demonstrate this phenomenon, showing the passage of an 8 nm diameter particle through a nanopore along two paths, as well as their associated current traces. To demonstrate this phenomenon, we placed the particle across a range of z positions (i.e. between 30 nm before the entrance and 30 nm after the exit of the nanopore), along two fixed lateral positions: central axis ($x = 0$) and off axis ($x = 11$ nm). The parameters used in this simulation are listed in table 2. The boundary conditions and initial values used in the Poisson and Nernst–Planck equations are listed in table 3. We calculated the total ionic current from the integration of ion fluxes across surface G indicated in table 3.

When the particle passes through the nanopore along the central axis, it produces a rounded resistive pulse shape due to gradual changes in access resistance at the entrance and exit of the pore (figure 2(b)). The off-axis passage, however, yields a square-shaped resistive pulse due to sharp changes in

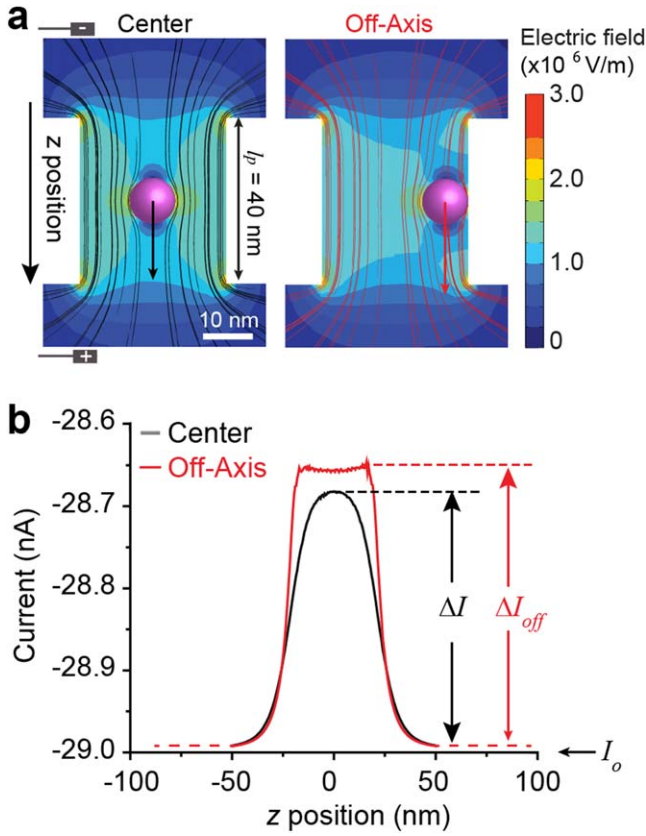


Figure 2. Influence of off-axis effects on a spherical particle translocating through a nanopore. (a) Electric field distribution in a nanopore when a particle with a diameter of 8 nm passes through the center (left) or off-axis (right). The fine lines represent the electric field. (b) The current as a function of the particle position when the particle transits through the center (black curve) and near the wall (red curve) of the nanopore. See supplementary video 1 for animations.

electric field at the corners of the pore. As expected, the blockade current for off-axis translocation, ΔI_{off} , is larger than the blockade current from translocation along the central axis, ΔI . We note that this observation is based on stationary study results, and therefore no particle dynamics are discussed.

The size of the nanopore relative to the size of the nanoparticle strongly influences the magnitude of off-axis effects. To quantify this influence, we allowed a spherical particle with a radius of 4 nm to pass through nanopores with varied radius, R_p , from 8 to 26.7 nm. We swept the radial distance x from zero (corresponding to the center) to the position $R_p - r$, where the nanoparticle touches the nanopore wall, as shown in figures 3(a) and (b). Figure 3(c) shows the distortion of the resistive-pulse magnitude, or deviation in $\Delta I/I_o$, for different off-axis positions of the spherical nanoparticle. These results calculated by finite element simulation agree with the analytical results reported by Houghtaling *et al* [22] and Qin *et al* [27]. As the particles translocated closer to the wall, we observed increasing deviations of $\Delta I/I_o$ especially in the case of small r/R_p ratios. In other words, off-axis effects are largest when small nanoparticles translocate near the wall of a large nanopore.

3.2. Off-axis translocation leads to overestimates of particle volume

Most approaches for characterizing particles and proteins with nanopores involve analyzing a population of resistive pulses [44]. In an ideal scenario, a population of identical, perfectly spherical particles would produce several resistive pulses of the same amplitude. Volume estimates of translocating particles are proportional to resistive-pulse amplitude, $\Delta I/I_o$, as expressed in equation (2), where γ equals 1.5 for a spherical shape. In practice, ensemble analyses are influenced by the recording noise of the experimental setup [49], which produces an approximately Gaussian distribution of resistive-pulse amplitudes. The experimental $\Delta I/I_o$ distribution can be viewed as the convolution of the recording noise and the theoretical resistive-pulse amplitude.

Figure 4 illustrates the off-axis effect on the measured $\Delta I/I_o$ distribution. We first determined the $\Delta I/I_o$ values by placing a nanoparticle at different distances from the central axis, as discussed in figure 3(c). Assuming that the particle is equally likely to be in any position inside a nanopore, we can randomly sample the position with a probability function $P(x)$. As illustrated in figure 4(a), $P(x)$ is the probability of finding a particle at a distance of $x + \Delta x$ from the center of the pore

$$P(x) = \frac{\Delta A}{A} = \frac{2x\Delta x}{(R_p - r)^2}, \quad (6)$$

where ΔA is the area of the band that could be occupied by the particle at that off-axis distance, and A represents the total possible cross-sectional area that the particle could sample inside the nanopore. After random sampling, we added normally distributed noise ($\mu = 0$, $\sigma = 25$ pA) to the each point of the simulation current [50], which is the typical level of rms current noise of a nanopore recording experiment at 15 kHz bandwidth [4, 43].

Figure 4(b) plots the PDF of the measured $\Delta I/I_o$ after considering the random spatial distribution and noise effect for the two extreme scenarios in figure 4(c). Compared to the PDFs in gray generated by central-axis translocation, off-axis translocation influences estimates of protein volume in two ways: (1) off-axis effects increase $\Delta I/I_o$ values and thus lead to an overestimation of the particle volume, and (2) the spread of the distribution of $\Delta I/I_o$ widens, which can produce errors in determining length-to-diameter ratios relative to reference values. Both of these consequences of off-axis translocation influence the accuracy of parameter estimates determined based on resistive pulses. Figure 4(c) shows the deviation of $\Delta I/I_o$, obtained by fitting the PDF with a Gaussian distribution function, as a function of the r/R_p ratio. Based on this deviation, we expect a 5% to 15% overestimation of volume if the particle is equally likely to be found in any given radial position within the nanopore, as described in equation (6).

Equation (6) assumes that the lateral diffusion of particles inside the nanopore is unbiased. This assumption, however, ignores the particle dynamics affected by Brownian motion, fluidic drag force and the electrophoretic force inside the nanopore. These forces will bias the particles toward the

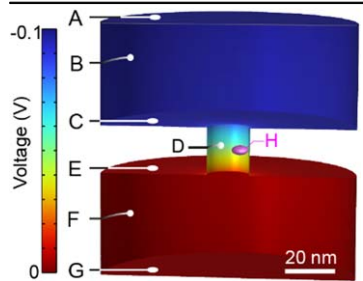
Table 1. Constants and parameters used for COMSOL Multiphysics simulation.

Parameters	Values	Details
z_K	1	The charge of K^+
z_{Cl}	-1	The charge of Cl^-
F	$96485 \text{ C}\cdot\text{mol}^{-1}$	Faraday constant
ε	80	Dielectric constant of the fluidic medium
R	$8.31 \text{ J}\cdot(\text{mol}\cdot\text{K})^{-1}$	Gas constant
T	295 K	Absolute temperature
D_K	$1.957 \times 10^{-9} \text{ m}^2\cdot\text{s}^{-1}$	Diffusion coefficient of K^+
D_{Cl}	$2.032 \times 10^{-9} \text{ m}^2\cdot\text{s}^{-1}$	Diffusion coefficient of Cl^-
Φ	-0.1 V	Applied voltage across the nanopore
c_i (K^+ or Cl^-)	1680 mol m^{-3}	Effective concentration of the K^+ and Cl^- ions according to the measured solution conductivity
L_p	40 nm	Length of the nanopore after coating
σ_{pore}	$0 \text{ mC}\cdot\text{cm}^{-2}$	Surface charge on the nanopore wall

Table 2. Parameters used for COMSOL Multiphysics simulation in figure 2.

Parameters	Values	Details
$d_{particle}$	8 nm	Diameter of the particles
$\sigma_{particle}$	$0 \text{ mC}\cdot\text{cm}^{-2}$	Surface charge density of the particles
Λ	268 nm^3	Volume of the particle
m	1.0	Length-to-diameter ratio m of the particle
x	0 nm for center 11 nm for off-axis	Radial distance from the particle center to the pore center
z	-50 nm to 50 nm	Particle position along the pore channel

Table 3. Boundary conditions for PNP equations.

	Surface	Poisson equation (equation (3))	Nernst-Planck equation (equation (4))
	A	Constant potential $V_p = -0.1 \text{ V}$	Concentration $c_i = 1.68 \text{ mol L}^{-1}$
	B, F	Zero charge, $n\cdot\nabla V = 0$	Insulation $n\cdot J = 0$
	C, D, E	Surface charge of the nanopore, 0	Insulation $n\cdot J = 0$
	H ^a	Surface charge of the particle, 0	Insulation $n\cdot J = 0$
	G ^b	Ground $V_0 = 0$	Concentration $c_i = 1.68 \text{ mol L}^{-1}$

^a No field interaction on particle surface H.

^b Ionic current is calculated from the integration of ion fluxes across surface G.

central axis [51], hence mitigating the off-axis effect. In addition to the particle dynamics, the simulation conducted here assumes a homogenous distribution of ions. All-atom molecular dynamics simulations, which provide a higher degree of accuracy than finite element simulations, have shown that the ion conductivity decreases to zero near the surface of the particle and the surface of the nanopore [52, 53]. The zero-conductivity zone around the particle leads to larger-than-expected resistive pulses when the particle translocates through the nanopore. When particles are at an off-axis position that is close to the nanopore surface,

however, the overlap of the zero-conductivity layers of the particle and the nanopore surface reduces the blockade current, thus mitigating the off-axis effect. From the above discussion, we expect a less pronounced overestimation of the particle's volume due to the off-axis effect in a true experiment in comparison to the simulated results presented here.

3.3. Off-axis effects on determination of a particle's ellipsoidal shape

Non-spherical particles rotate as they translocate through the nanopore, and these rotations produce characteristic

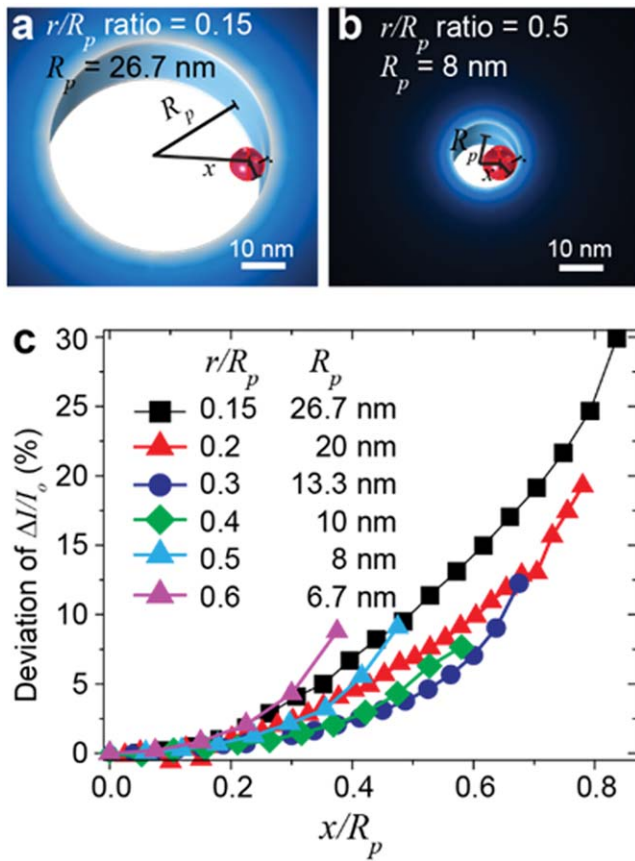


Figure 3. Influence of the ratio between particle size and nanopore size on off-axis effects. (a) Illustration of a small r/R_p ratio, showing a nanopore with a radius of 26.7 nm and a particle with a radius of 4 nm. (b) Illustration of a large r/R_p ratio, showing a nanopore with a radius of 8 nm and a particle with a radius of 4 nm. (c) Deviation of $\Delta I/I_0$ as a function of normalized radial position, x/R_p . The radius of the spherical nanoparticle is fixed ($r = 4$ nm), while the radius of the nanopore, R_p , varies from 6.7 to 26.7 nm.

fluctuations in the associated resistive pulse [4, 22, 27, 54]. Figure 5(a) shows the fluctuations within a resistive pulse caused by different orientations of ellipsoidal particles with the same volume but different length-to-diameter ratios. The particles pass through a nanopore while rotating at a constant step (0.28 nm, 10° per step), which imposes periodicity in the fluctuations of blockade current. The ratio of maximum to minimum blockade current, $\Delta I_{\max}/\Delta I_{\min}$, can be used to estimate the particle's ellipsoidal shape, as shown in figure 5(b). When a sphere transits through a nanopore while oscillating in lateral position between opposite sides of the pore (see supplementary video 2), the blockade current, represented by the red curve in figure 5(a), exhibits oscillations similar to those generated by a prolate and oblate (supplementary video 3). In other words, the fluctuations due to off-axis effects from a perfectly spherical particle could lead to an erroneous shape estimation that deviates from that of a sphere ($m = 1$).

In addition, the shape and orientation of a translocating particle dictate the range of possible deviations in its radial position, which in turn influence the shape predicted from its current trace. In previous work we showed that this

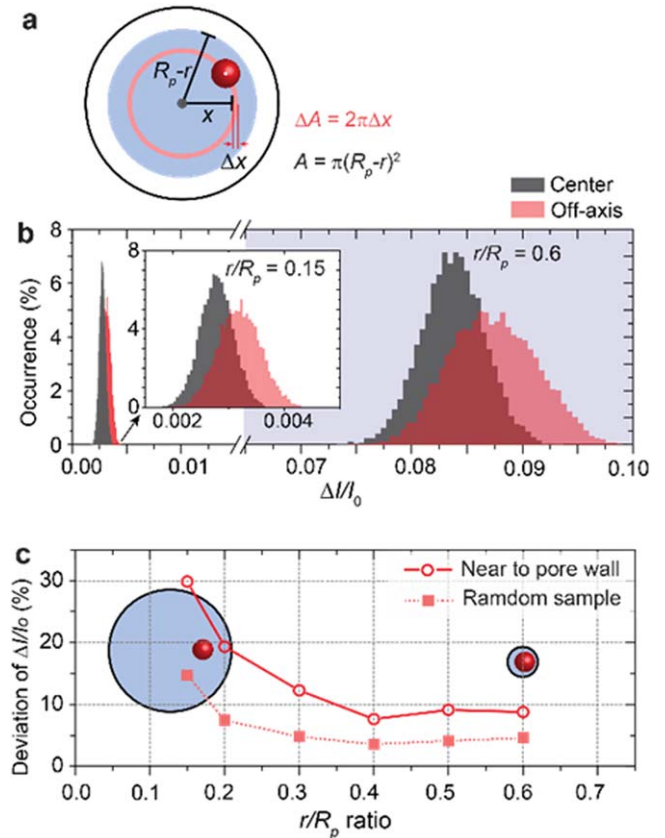


Figure 4. Effects of off-axis translocation on population-based analysis of particle volume. (a) Schematic cross section representing possible locations of a particle at a given off-axis position inside a nanopore (b) The probability distribution (PDF) of predicted $\Delta I/I_0$ values with (pink) and without (gray) considering off-axis effects from randomly sampled positions. (c) Deviation of $\Delta I/I_0$ as a function of the r/R ratio. The insets represent the situation of a particle with a radius of 4 nm inside a nanopore with a radius of 26.7 nm (left inset, $r/R_p = 0.15$), or inside a nanopore with a radius of 6.65 nm (right inset, $r/R_p = 0.6$).

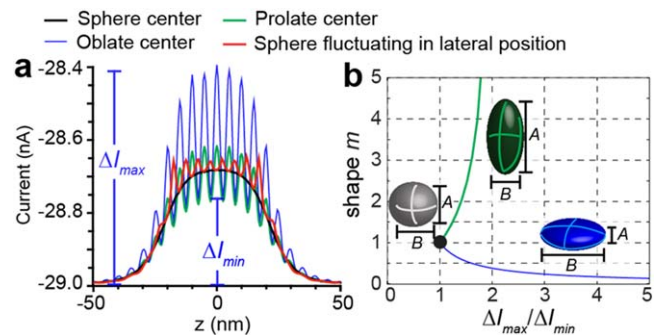


Figure 5. Effects of maximum and minimum blockade current on the determination of the ellipsoidal shape of particles. (a) Simulated current as a function of the particle position along the nanopore length when particles of the same volume (268 nm³) but different shape and orientation transit through a nanopore. The ΔI_{\max} and ΔI_{\min} are the maximum and the minimum blockade current when the particle is in the middle of the nanopore channel (i.e. $z = 0$). (b) Determination of length-to-diameter ratio using $\Delta I_{\max}/\Delta I_{\min}$ with ΔI_{\max} and ΔI_{\min} indicated in panel a and equations 14 and 15 in supplementary information of [4].

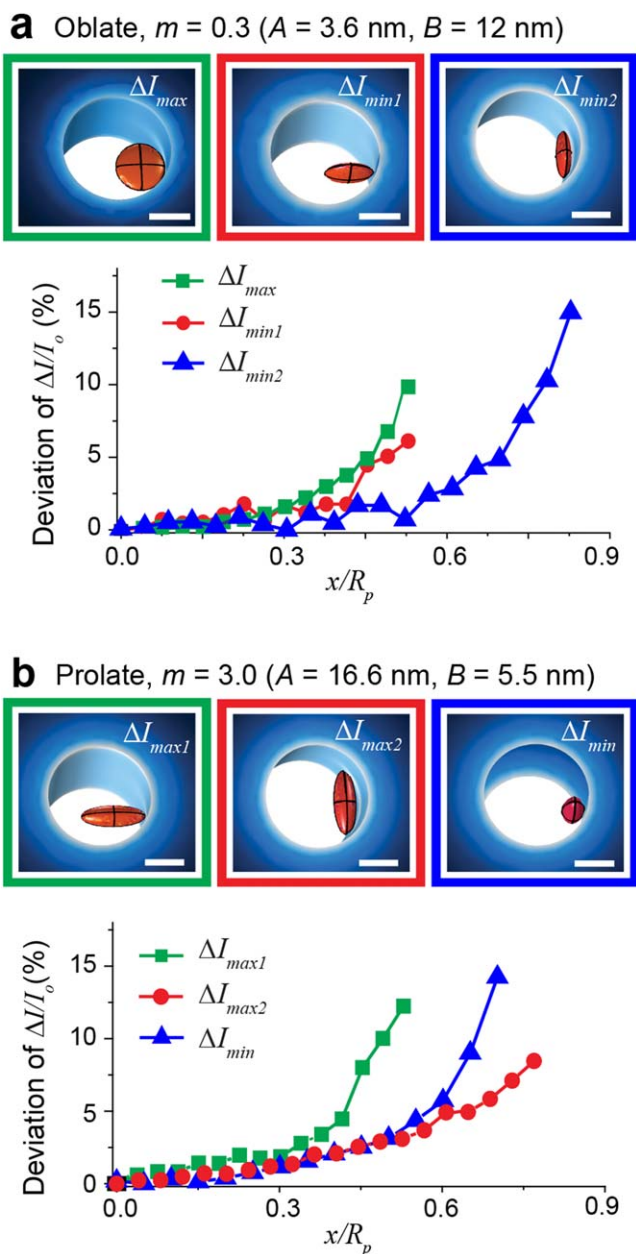


Figure 6. Effects of off-axis translocation on $\Delta I/I_0$ for non-spherical particles in different orientations. (a) Oblate particles have two minimum orientations, and can produce more than 15% deviation in $\Delta I/I_0$ in the most extreme case (blue box and curve). (b) Prolate particles have two maximum orientations, and can distort $\Delta I/I_0$ by 15% in their most extreme minimum orientation (blue box and curve). The nanopore radius for these simulations was 13.35 nm, the particles' volume was 268 nm³, and the r/R ratio equalled 0.3. The scale bars are 10 nm.

orientation-dependent off-axis effect could influence shape determination [22]. Figure 6 shows oblate and prolate particles of the same volume translocating in their γ_{\min} and γ_{\max} orientations through a nanopore. Due to symmetry, oblate particles exhibit two orientations with minimum cross-sectional area, henceforth referred to as minimum orientation. In contrast, prolate particles occupy two orientations with maximum cross-sectional area, henceforth referred to as maximum orientation. These two minimum (oblate) or

maximum (prolate) orientations produce the same blockade current when particles transit through a nanopore along its central axis. When considering the off-axis effect, however, these two orientations could lead to different extreme off-center positions due to their differences in curvature (see the example of an oblate transiting through a nanopore at its two maximum orientations in supplementary video 4). Figure 6 illustrates different scenarios for three extreme orientations of both an oblate and a prolate, as well as the deviation of measured $\Delta I/I_0$ as a function of the off-axis position. As the particle approaches the pore wall, the deviation of $\Delta I/I_0$ increases for each orientation. The maximum deviation in $\Delta I/I_0$ appears when sampling the minimum orientations for both oblates and prolates, because these two orientations allow the smallest distance between the center of the particle and the pore wall. These deviations in $\Delta I/I_0$ lead to uncertainty in the protein's shape evaluation when performing resistive pulse-based nanopore sensing.

To estimate the possible uncertainty that could be generated due to off-axis effects, we considered two extreme scenarios for each particle shape and r/R ratio by simulation: maximum ΔI_{\max} in combination with minimum ΔI_{\min} , and minimum ΔI_{\max} in combination with maximum ΔI_{\min} . These two scenarios lead to the boundaries of the gray area shown in figure 7. The gray areas represent the possible deviation of the estimated shapes from true shapes for different particle-to-pore size ratios, ranging from 0.15 to 0.4. When the particle-to-pore size ratio is small, the estimated shape for a prolate could deviate multiple fold from its real shape, as shown in figure 7(a). This estimation represents the extreme errors one can expect from off-axis effects. On the other hand, when selecting a nanopore with a diameter close to the size of the particle (while still allowing the particle to rotate freely), the estimated shapes are close to the actual particle shape. Estimates for oblates are within 5% of their actual shape, while estimates for extreme prolates are within 20% (figure 7(d)). Previous experimental observations confirm that the estimated shape of free translocated proteins is within 20% deviation from their true shape (figure 3(B) in [22]).

In previous work [4], we employed crosslinkers to tether proteins to a fluid lipid-bilayer coating on the nanopore wall. This tether keeps proteins close to the pore wall at all times. We estimated the shape in such a scenario for different particle-to-pore size ratios, as represented by the red circles in figure 7. We found that tethering particles to the nanopore walls improves estimates of shape relative to freely translocating particles. The largest deviations from true shape values in both tethered and untethered translocations occur when the pore is much larger than the protein, or when the particle has a relatively extreme prolate shape.

Note that figure 7 assumes no bias in the orientation or lateral diffusion of the particles translocating through the nanopore. In reality, particles with a permanent dipole moment may not rotate randomly while passing through the nanopore; instead, the electric field acts on the particle's dipole moment and tends to align the particle's longest axis parallel to the local electric field [51, 55]. Ai and Qian reported that when the flow field and electrophoretic force are

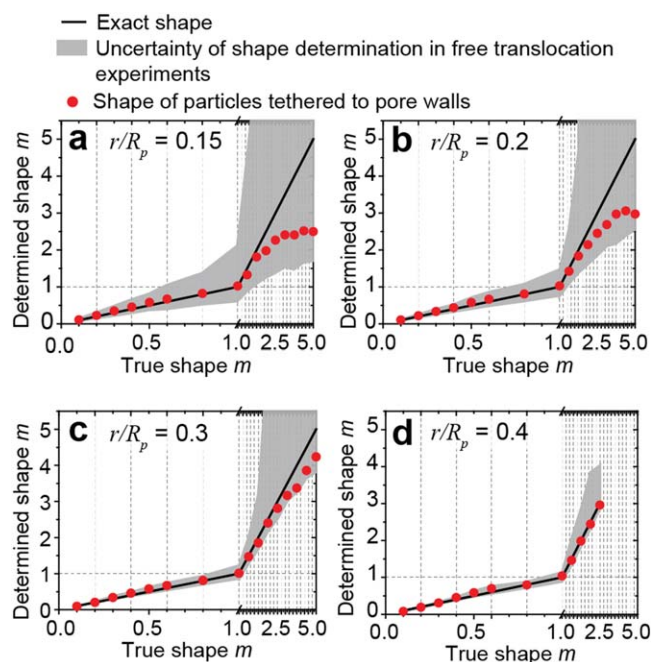


Figure 7. Effect of off-axis translocation on the estimation of a particle's shape, expressed as length-to-diameter ratio, m . (a)–(d) Simulated and true shapes for different particle-to-pore size ratios, ranging from 0.15 to 0.4. The gray areas represent the uncertainty of shape determination for free translocations, and the red circles represent the estimated shapes when particles are tethered to the pore walls. For the tethered simulations, we fixed the minimal distance between the edge of the particle and the nanopore to 0.2 nm.

taken into account, particles tend to translocate along the central axis at their minimal orientations [51]. In this scenario, off-axis translocation leads to an extreme estimation of shape, m_{est} , compared to the true shape, m_0 , (i.e. $m_{est} < m_0$ for oblates and $m_{est} > m_0$ for prolates). This conclusion agrees with our previous experimental observation reported in [22]. Interestingly, when the electric field is relatively low ($2 \times 10^4 \text{ V m}^{-1}$), the initial orientation of a particle above the nanopore entrance can influence the lateral movement of the particle [51]. When the longest axis of the particle is misaligned with respect to the center axis of the nanopore, it rotates before entering the nanopore and at the same time moves laterally [51, 55]. This orientational and lateral adjustment during the capture dynamics could slow down an ellipsoid while it approaches the nanopore, hence increasing the time to capture. Therefore, we expect a higher order of randomness in the capture time for ellipsoids compared to spherical particles.

4. Conclusion

Off-axis effects produce larger-than-expected estimates of particle volume in resistive-pulse experiments, which can result in error in estimates of length-to-diameter ratio. Selecting a nanopore with a diameter that is as small as possible while still allowing the particle to fully rotate within the pore minimizes off-axis effects; in this case, the estimated shape falls within 5% of the actual particle shape in most cases, with

no more than a 20% discrepancy in the case of extreme particle shapes. Tethering nanoparticles to fluid coatings on the nanopore wall mitigates the effects of off-axis translocation on estimates of nanoparticle shape, in particular for particles with shape values between $m = 0.1$ and $m = 2.0$ [4].

Acknowledgments

This research was supported by Oxford Nanopore Technologies (M.M., Grant Number 350509-N016133), the Swiss National Science Foundation (SNSF), Grant No. 200021_169304 and Grant No. 200020_197239 to M.M.

Data availability statement

The data that support the findings of this study are available upon reasonable request from the authors.

ORCID iDs

Cuifeng Ying  <https://orcid.org/0000-0002-7279-1388>
 Jared Houghtaling  <https://orcid.org/0000-0003-1557-9716>
 Michael Mayer  <https://orcid.org/0000-0002-6148-5756>

References

- [1] Graham M 2003 The Coulter principle: foundation of an industry *J. Assoc. Lab. Autom.* **8** 72–81
- [2] Dekker C 2007 Solid-state nanopores *Nat. Nanotechnol.* **2** 209–15
- [3] Oukhaled A, Bacri L, Pastoriza-Gallego M, Betton J M and Pelta J 2012 Sensing proteins through nanopores: fundamental to applications *ACS Chem. Biol.* **7** 1935–49
- [4] Yusko E C *et al* 2017 Real-time shape approximation and fingerprinting of single proteins using a nanopore *Nat. Nanotechnol.* **12** 360–7
- [5] Clarke J, Wu H C, Jayasinghe L, Patel A, Reid S and Bayley H 2009 Continuous base identification for single-molecule nanopore DNA sequencing *Nat. Nanotechnol.* **4** 265–70
- [6] Schneider G F and Dekker C 2012 DNA sequencing with nanopores *Nat. Biotechnol.* **30** 326–8
- [7] Xue L, Yamazaki H, Ren R, Wanunu M, Ivanov A P and Edell J B 2020 Solid-state nanopore sensors *Nat. Rev. Mater.* **5** 931–51
- [8] Drndić M 2021 20 years of solid-state nanopores *Nat. Rev. Phys.* **1** 606
- [9] Li J, Yu D and Zhao Q 2015 Solid-state nanopore-based DNA single molecule detection and sequencing *Microchim. Acta* **183** 941–53
- [10] Lee K, Park K B, Kim H J, Yu J S, Chae H, Kim H M and Kim K B 2018 Recent progress in solid-state nanopores *Adv. Mater.* **30** 1704680
- [11] Brinkerhoff H, Kang A S W, Liu J, Aksimentiev A and Dekker C 2021 Multiple rereads of single proteins at single-amino acid resolution using nanopores *Science* **1513** 1509–13
- [12] Hu R *et al* 2018 Differential enzyme flexibility probed using solid-state nanopores *ACS Nano* **12** 4494–502

- [13] Alfaro J A *et al* 2021 The emerging landscape of single-molecule protein sequencing technologies *Nat. Methods* **18** 604–17
- [14] Houghtaling J, List J and Mayer M 2018 Nanopore-based, rapid characterization of individual amyloid particles in solution: concepts, challenges, and prospects *Small* **14** e1802412
- [15] Arima A *et al* 2018 Identifying single viruses using biorecognition solid-state nanopores *J. Am. Chem. Soc.* **140** 16834–41
- [16] Darvish A *et al* 2019 Mechanical characterization of HIV-1 with a solid-state nanopore sensor *Electrophoresis* **40** 776–83
- [17] Leong I W, Tsutsui M, Yokota K and Taniguchi M 2021 Salt gradient control of translocation dynamics in a solid-state nanopore *Anal. Chem.* **93** 16700–8
- [18] DeBlois R W and Bean C P 1970 Counting and sizing of submicron particles by the resistive pulse technique *Rev. Sci. Instrum.* **41** 909–16
- [19] DeBlois R W, Uzgiris E E, Cluxton D H and Mazzone H M 1978 Comparative measurements of size and polydispersity of several insect viruses *Anal. Biochem.* **90** 273–88
- [20] Golibersuch D C 1973 Observation of aspherical particle rotation in poiseuille flow via the resistance pulse technique *Biophys. J.* **13** 265–80
- [21] Garboczi E J 2017 The influence of particle shape on the results of the electrical sensing zone method as explained by the particle intrinsic conductivity *Powder Technol.* **322** 32–40
- [22] Houghtaling J, Ying C, Eggenberger O M, Fennouri A, Nandivada S, Acharjee M, Li J, Hall A R and Mayer M 2019 Estimation of shape, volume, and dipole moment of individual proteins freely transiting a synthetic nanopore *ACS Nano* **13** 5231–42
- [23] Sha J, Si W, Xu B, Zhang S, Li K, Lin K, Shi H and Chen Y 2018 Identification of spherical and nonspherical proteins by a solid-state nanopore *Anal. Chem.* **90** 13826–31
- [24] Acharya S, Jiang A, Kuo C, Nazarian R, Li K, Ma A, Siegal B, Toh C and Schmidt J J 2020 Improved measurement of proteins using a solid-state nanopore coupled with a hydrogel *ACS Sens.* **5** 370–6
- [25] Zhang M, Chen S, Hu J, Ding Q, Li L, Lü S and Long M 2021 Mapping the morphological identifiers of distinct conformations: Via the protein translocation current in nanopores *Nanoscale* **13** 6053–65
- [26] Smythe W R 1972 Off-axis particles in coulter type counters *Rev. Sci. Instrum.* **43** 817–8
- [27] Qin Z, Zhe J and Wang G-X 2011 Effects of particle's off-axis position, shape, orientation and entry position on resistance changes of micro Coulter counting devices *Meas. Sci. Technol.* **22** 45804
- [28] Berge L I, Jossang T and Feder J 1990 Off-axis response for particles passing through long apertures in Coulter-type counters *Meas. Sci. Technol.* **1** 471
- [29] Hinkle P, Westerhof T M, Qiu Y, Mallin D J, Wallace M L, Nelson E L, Taborek P and Siwy Z S 2017 A hybrid resistive pulse-optical detection platform for microfluidic experiments *Sci Rep.* **7** 10173
- [30] Kowalczyk S W, Grosberg A Y, Rabin Y and Dekker C 2011 Modeling the conductance and DNA blockade of solid-state nanopores *Nanotechnology* **22** 315101
- [31] Rollings R, Graef E, Walsh N, Nandivada S, Benamara M and Li J 2015 The effects of geometry and stability of solid-state nanopores on detecting single DNA molecules *Nanotechnology* **26** 44001
- [32] Davenport M, Healy K, Pevarnik M, Teslich N, Cabrini S, Morrison A P, Siwy Z S, Letant S E and Létant S E 2012 The role of pore geometry in single nanoparticle detection *ACS Nano* **6** 8366–80
- [33] Liu J, Kvetny M, Feng J, Wang D, Wu B, Brown W and Wang G 2012 Surface charge density determination of single conical nanopores based on normalized ion current rectification *Langmuir* **28** 1588–95
- [34] Jiang Z and Stein D 2011 Charge regulation in nanopore ionic field-effect transistors *Phys. Rev. E* **83** 031203
- [35] Wen C, Zhang Z and Zhang S L 2017 Physical model for rapid and accurate determination of nanopore size via conductance measurement *ACS Sens.* **2** 1523–30
- [36] Pham N H, Yao Y, Wen C, Li S, Zeng S, Nyberg T, Tran T T, Primetzhofer D, Zhang Z and Zhang S-L 2021 Self-limited formation of bowl-shaped nanopores for directional DNA translocation *ACS Nano* **15** 17938–46
- [37] Chuah K, Wu Y, Vivekchand S R C, Gaus K, Reece P J, Micolich A P and Gooding J J 2019 Nanopore blockade sensors for ultrasensitive detection of proteins in complex biological samples *Nat. Commun.* **10** 1–9
- [38] Yilmaz D, Kaya D, Keçeci K and Dinler A 2020 Effects of asymmetric nanopore geometries on nanoparticle sensing using track-etched nanopore membranes *Haceteppe J. Biol. Chem.* **49** 207–17
- [39] Brown A S and MacInnes D A 1935 The determination of activity coefficients from the potentials of concentration cells with transference. I. Sodium chloride at 25 *J. Am. Chem. Soc.* **57** 1356–62
- [40] Ying C, Houghtaling J, Eggenberger O M, Guha A, Nirmalraj P, Awasthi S, Tian J and Mayer M 2018 Formation of single nanopores with diameters of 20–50 nm in silicon nitride membranes using laser-assisted controlled breakdown *ACS Nano* **12** 11458–70
- [41] Wang J, Ma J, Ni Z, Zhang L and Hu G 2014 Effects of access resistance on the resistive-pulse caused by translocating of a nanoparticle through a nanopore *RSC Adv.* **4** 7601
- [42] Eggenberger O M, Ying C and Mayer M 2019 Surface coatings for solid-state nanopores *Nanoscale* **11** 19636–57
- [43] Awasthi S *et al* 2020 Polymer coatings to minimize protein adsorption in solid-state nanopores *Small Methods* **4** 2000177
- [44] Yusko E C, Johnson J M, Majd S, Prangkio P, Rollings R C, Li J, Yang J and Mayer M 2011 Controlling protein translocation through nanopores with bio-inspired fluid walls *Nat. Nanotechnol.* **6** 253–60
- [45] Schmid S and Dekker C 2021 The NEOTrap—en route with a new single-molecule technique *iScience* **24** 103007
- [46] Galla L, Meyer A J, Spiering A, Sischka A, Mayer M, Hall A R, Reimann P and Anselmetti D 2014 Hydrodynamic slip on DNA observed by optical tweezers-controlled translocation experiments with solid-state and lipid-coated nanopores *Nano Lett.* **14** 4176–82
- [47] Shen K H and Hall L M 2020 Ion conductivity and correlations in model salt-doped polymers: effects of interaction strength and concentration *Macromolecules* **53** 3655–68
- [48] Saleh O A and Sohn L L 2002 Correcting off-axis effects in an on-chip resistive-pulse analyzer *Rev. Sci. Instrum.* **73** 4396–8
- [49] Uram J D, Ke K and Mayer M 2008 Noise and bandwidth of current recordings from submicrometer pores and nanopores *ACS Nano* **2** 857–72
- [50] Raimund O, Caves J and Ward E S 2003 Analysis of exponential data using a noniterative technique: application to surface plasmon experiments *Anal. Biochem.* **312** 57–65
- [51] Ai Y and Qian S 2011 Electrokinetic particle translocation through a nanopore *Phys. Chem. Chem. Phys.* **13** 4060–71
- [52] Wilson J, Sarthak K, Si W, Gao L and Aksimentiev A 2019 Rapid and accurate determination of nanopore ionic current using a steric exclusion model *ACS Sens.* **4** 634–44
- [53] Si W and Aksimentiev A 2017 Nanopore sensing of protein folding *ACS Nano* **11** 7091–100
- [54] Szuttor K, Kreissl P and Holm C 2021 A numerical investigation of analyte size effects in nanopore sensing systems *J. Chem. Phys.* **155** 134902
- [55] Chinappi M, Yamaji M, Kawano R and Cecconi F 2020 Analytical model for particle capture in nanopores elucidates competition among electrophoresis, electroosmosis, and dielectrophoresis *ACS Nano* **14** 15816–28